ACES Asian Chemical Editorial Society

DOI: 10.1002/cnma.201900035

CHEMNANOMAT
Full Paper

Spot-on SERS Detection of Biomolecules with Laser-Patterned Dot Arrays of Assembled Silver Nanowires

Martina Banchelli,[a] Chiara Amicucci,[a, e] Emmanuel Ruggiero,[a, c] Cristiano D'Andrea,[a] Maximilien Cottat,[a, d] Daniele Ciofini,[a] Iacopo Osticioli,[a] Giacomo Ghini,[b] Salvatore Siano,[a] Roberto Pini,[a] Marella de Angelis,[a] and Paolo Matteini*[a]

Abstract: Unique characteristics of SERS including the possibility to reveal the compositional and structural content of trace amounts of biological samples without any pre-treatment, depict this technique as a promising label-free alternative to standard analytical methods. Despite significant advancements, current SERS substrates for biomolecule detection suffer from a number of issues still impeding their routine usage and commercial exploitation, including complex and expensive fabrication procedures and scarce standardization perspectives. Herein a combined bottom up/top down scheme based on flow-through method plus laser patterning is proposed to prepare dot arrays of silver nanowires on a hydrophobic substrate for catching the analyte content from a minute amount of liquid sample and its rapid SERS inspection. As a consequence, a simple spot-on analysis specifically adapted for reliable identification and characterization of molecules of biomedical interest is made possible. Our attempt may represent a concrete chance for progressing SERS toward widespread commercially viable sensing applications including diagnostics at the point-of-need settings and on-site analyses.

1. Introduction

Plasmonic substrates (e.g. substrates supporting localized surface plasmon resonances featured by nanoscaled metallic surfaces or assembled nanoparticles) for surface-enhanced Raman scattering (SERS) analyses require abiding by a number of key needs in order to find effective application in basic research. These primarily include enough sensitivity and high reproducibility, which nowadays have been mostly implemented in a large variety of SERS substrates as a result of the recent great advances in nanofabrication techniques.[1–3] However additional aspects shall be considered when dealing with daily life applications. These include low production costs, fabrication methods suitable for high volume manufacturing, reduced training times and skills needed for their routine usage, integration potential with portable Raman systems for on site applications, simple reusage or disposable characteristics and quick processing of a variety of samples.[4–7]

The above considerations hold particular significance when life science and healthcare applications of SERS are concerned,[8,9] whose primary conditions are high-throughput, multisample and inexpensive analyses at reduced costs.[10,11] According to this picture, in the last decade a great deal of efforts has been exerted in the development of functional SERS substrates obtained by simple, low cost, rapid and scalable fabrication methods, such as micropipetting, screen- and ink-jet printing, and filtration of colloidal solutions of plasmonic nanoparticles.[12–16]

Concerning biomolecule detection, previous tests at the laboratory level have been mainly based on adding a biomolecule solution to a dispersion of noble metal colloidal nanoparticles. By adding aggregating agents or imparting the particle with suitable surface charge, the formation of inter-particle gaps enclosing adsorbed molecules is induced.[17,18] Upon excitation with appropriate light, the Raman signal of an adsorbed species in the gaps is amplified to such an extent to provide characteristic fingerprint information. In this case, the formation of particle clusters with highly divergent size causes scarce reproducibility with large signal variability,[19–22] which remains a main obstacle of this approach. Alternative strategies have been recently aimed at obtaining more consistent and dependable SERS responses from biomolecules. Relevant examples are the SERS detection of proteins adsorbed at specific sites on the surface of nanocrystals showing highly localized electromagnetic fields[23] or by gathering molecules in spatial proximity to SERS hotspots generated at the junctions among

[a] Dr. M. Banchelli, Dr. C. Amicucci, Dr. E. Ruggiero, Dr. C. D'Andrea, Dr. M. Cottat, Dr. D. Ciofini, Dr. I. Osticioli, Dr. S. Siano, Prof. R. Pini, Dr. M. de Angelis, Dr. P. Matteini
IFAC-CNR
Institute of Applied Physics "Nello Carrara"
National Research Council
Via Madonna del Piano 10, 50019 Sesto Fiorentino, Italy
E-mail: p.matteini@ifac.cnr.it

[b] Dr. G. Ghini
Cabro S.p.A.
Via Setteponti 141, 52100 Arezzo, Italy

[c] Dr. E. Ruggiero
BASF SE
Carl-Bosch-Str. 38, 67056 Ludwigshafen am Rhein, Germany

[d] Dr. M. Cottat
Laboratoire des Technologies et de la Microélectronique
CNRS, 17
avenue des martyrs (CEA-LETI), 38054 Grenoble Cedex, France

[e] Dr. C. Amicucci
Department of Industrial Engineering, University of Florence, via Santa Marta 3, 50134 Florence, Italy

Supporting information for this article is available on the WWW under https://doi.org/10.1002/cnma.201900035

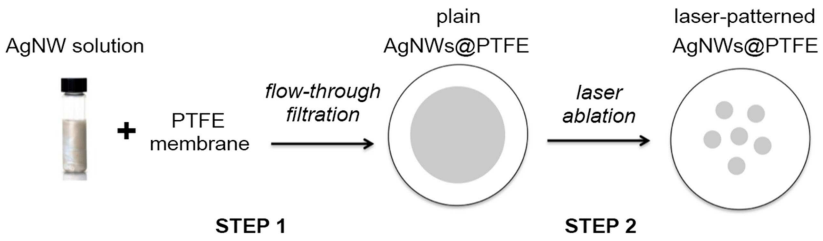

Figure 1. Scheme of the bottom-up/top-down fabrication process for preparing the SERS substrates. Initially an alcoholic solution of AgNWs is filtered through a PTFE filter membrane (STEP 1). Afterwards, laser ablation is used for patterning the substrate (STEP 2).

optically-aggregated plasmonic nanoparticles.[24] Despite significant advancements, the above efforts remain of limited applicability in light of a forthcoming sustainable production and commercial exploitation. Nowadays, growing expectations are being set towards more reliable SERS substrates specifically created for practical detection of molecules of biomedical significance to be used close to or at the point-of-need settings.[25,26] Nonetheless, their effective realization remains largely underexplored.

In this work we demonstrate the possibility to take advantage of rapid, inexpensive fabrication techniques to produce disposable SERS substrates that can be integrated with a simple spot-on analysis specifically adapted for reliable detection and characterization of molecules of biomedical interest. Precisely, by combining the self-assembly of filtered nanowires and control over their cluster density with the laser ablation removal of predetermined areas from the SERS-active layer, ordered and spatially confined plasmonic spots accommodating a high concentration of molecules are obtained. This novel design approach, which integrates the strengths of bottom-up and top-down strategies, promotes synergic effects conferring efficiency to the system in such a way to overcome the capabilities of existing label-free SERS methods for biomolecule detection.

2. Results and Discussion

A primary obstacle toward setting up a SERS assay for biomolecule detection is represented by their low Raman cross-section, which is less than 10^{-30} cm^2 per molecule.[27] This value is well below that of a standard SERS probe such as rhodamine 6G, in both resonant (10^{-25} cm^2) and nonresonant (10^{-27} cm^2) conditions.[28] Moreover, biomolecules in their own biological environments are found in highly diluted (micromolar and below) concentration.[29] Thus, in order to capture enough SERS signal from the biomolecule content of a biological sample, increasing the local molecular density at SERS-sensitive sites[30,31] or using structures with sharp nanoscaled protrusions or tips featuring intense E-fields[32,33] are amongst the most convenient approaches. Here, we tried to capitalize on both these aspects aimed at assuring as well the fundamental prerequisites of SERS substrates for widespread use. For this purpose we focused on silver nanowires (AgNWs) that are one dimensional high-aspect ratio rod-like nanoparticles, which have recently attracted the interest, among others, of the sensing community due to their large surface area and possibility to easily manipulate and arrange them in 2D or 3D assemblies.[6,34,35]

We employed a revised polyol process to produce ~1.5 μm-long, 80 nm-thick PVP-capped AgNWs (Figure S1a, Supporting Information). These particles show characteristics LSPR bands at 349 nm and 380 nm (Figure S1b, Supporting Information), which can be assigned to the transverse modes. Additional extinction in the red-NIR region can be attributed to longitudinal plasmons.[36] The AgNWs were assembled on commercial filter membranes *via* simple flow-through method, which appears as a convenient tool for rapid realization of SERS-active substrates by using low-cost equipment available in a standard laboratory setting. Our choice of membrane type was aimed at favouring the molecule-metal surface interaction in order to capture the signal from the highest number of biomolecules in the sample. Thus, a disposable hydrophobic PTFE filter membrane (25 mm diameter × 80 μm thickness, 0.45 μm pore size) was selected to serve this purpose: it shows a water contact angle $\geq 90°$ that optimally satisfy the requirements shown by a hydrophobic surface to driving molecules toward sensitive areas overcoming the diffusion limit.[37,38] Upon passing the colloidal AgNWs solution through the membrane, a 12.5 mm-wide deposition of wires intertwined on the top of the PTFE surface is formed (Figure 1, step 1). In an attempt to optimize the SERS signal we varied the number of AgNWs loaded on the surface of the membrane by subsequent dilutions of the particle dispersion. Tests of the response at different density of the AgNWs on the PTFE surface were carried out on myoglobin (Mb, $M_w = 16.7$ kDa), a 3.5 nm in size common cardiac protein biomarker frequently taken as model biomolecule in Raman studies.[39] We were able to detect intense SERS signals from 5 μL single drops of a 1×10^{-6} M aqueous solution of Mb deposited on the surface of the substrate and left dry (Figure 2a).

An abrupt increase of protein signals was observed by halving twice the initial AgNW surface density, *i.e.* 0.4 μg/mm^2, down to final 0.1 μg/mm^2. Conversely, after further dilution of deposited AgNWs, the protein signals progressively lose intensity before completely disappearing at values below 0.01 μg/mm^2, where PTFE signals start prevailing. On increasing the number of nanowires, increased SERS intensity values are expected due to a larger number of hotspots in the focal

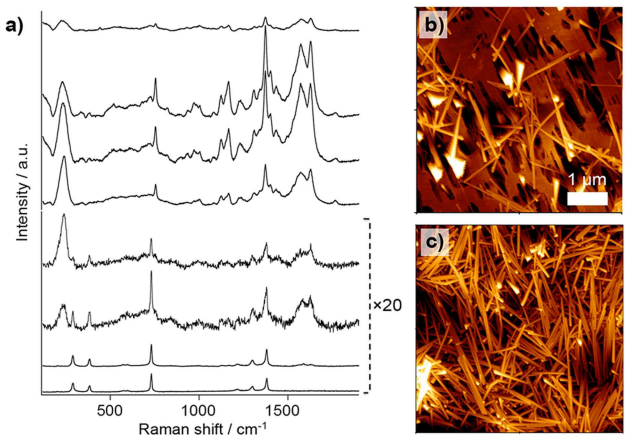

Figure 2. (a) SERS spectra ($\lambda_{ex}=532$ nm) of Mb (1×10^{-6} M) on AgNWs@PTFE substrates at different surface density values of AgNWs: from top to bottom, 0.4, 0.2, 0.1, 0.04, 0.02, 0.01, 0.004, 0 (pure PTFE) µg/mm^2. At low AgNW density values ($\leq$0.02 µg/mm^2) PTFE peaks at 734 cm^{-1} and 1382 cm^{-1} appear close to Mb peaks at 755 cm^{-1} and 1372 cm^{-1}. AFM images of AgNWs@PTFE substrates at 0.1 µg/mm^2 (b) and 0.4 µg/mm^2 (c) AgNW density.

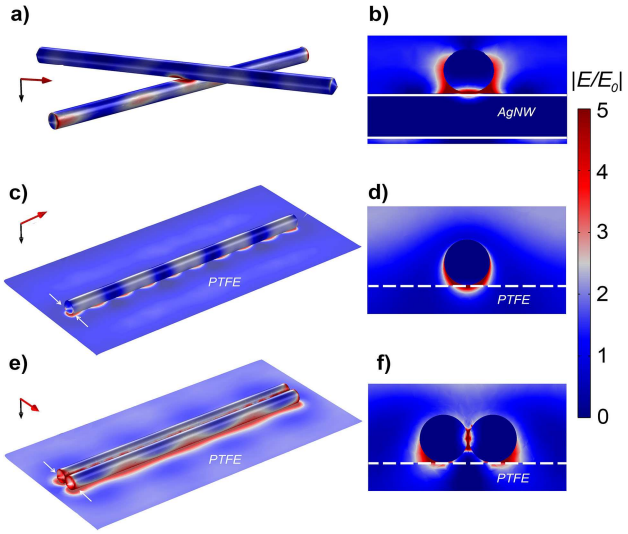

Figure 3. FEM simulations of the E-field intensity in-between two crossed AgNWs in air (a); in the proximity of an AgNW laying on a PTFE surface (c); within two bundled AgNWs laying on a PTFE surface (e). The configurations providing maximum E-field intensities are visualized. 2D sections of (a), (c) and (e) calculated at the junction between nanowires (b) or nearby the ends of the nanowires (arrows in (c,e)) are also reported.

volume mainly originated from wire extremities and contact points.[40] The above statement holds true from 0.004 µg/mm^2 until the optimal 0.1 µg/mm^2 of AgNWs, the latter corresponding to isolated or randomly clustered nanowires over the membrane (Figure 2b) with an estimated particle density of about 25×10^6 AgNWs/mm^2.

Beyond this optimal value, the SERS signal intensity decreases, reaching minimal values at 0.4 µg/mm^2. In the case of a high surface density of wires, two main causes influence the drop in Raman signal. First, a 3D arrangement of nanowires becomes apparent (Figure 2c) and the substrate experiences a change in its wettability abandoning the typical hydrophobic behaviour of PTFE. As a consequence, while a higher hotspot density per unit volume should produce higher SERS signals, protein molecules spread over a larger Ag surface (Figure S2, Supporting Information), causing a lowered SERS response. Additionally, internal hotspots are shielded by more exposed nanostructures and might not contribute to the final SERS signal.[2]

Further insight into the SERS response of the AgNWs@PTFE substrate was obtained by a theoretical simulation of the E-field distribution. The largest E-field value was found at the junctions between AgNWs and quantified as $|E|/|E_0|\sim5.3$ within a volume at the interface between two crossed AgNWs (Figures 3a,b). By careful inspection of AFM topographies (Figure S3a, Supporting Information), we may note that this configuration is experienced by at least 80% of the wires. Other less common configurations include isolated and bundled AgNWs laying on the PTFE surface. We estimated an $|E|/|E_0|\sim3.5$ in a volume in-between a single wire and the PTFE surface, which is justified by a LSPR coupling with the dielectric substrate (Figure 3c),[41] being optimal at the extremities of the wire (Figure 3d). When bundled AgNWs on PTFE are considered (Figure 3e), the hotspot generated along the intersection prevails (Figure 3f), resulting in $|E|/|E_0|\sim4.5$ In summary, the SERS intensity follows the order:

$$I_{crossed} > I_{bundle@PTFE} > I_{isolated@PTFE} > I_{tip.}$$

This result reveals a localization of the strongest fields at interstitials between AgNWs. These have been previously indicated as mainly responsible of the SERS activity of AgNW assemblies showing a SERS enhancement surpassing that of the isolated counterpart due to a strong plasmon coupling effect.[42] At the same time, the influence of the supporting material in altering the E-field distribution is brought to light, resulting in asymmetric localized plasmons confined at nanoparticle/dielectric gap.[43] Although the larger space available for molecular adsorption and detection provided by the hotspots within bundled AgNWs and at the AgNWs/PTFE junctions with respect to those inside crossed AgNWs, the prevalence of the latter in the AgNW assemblies suggests that it will largely govern the Raman enhancement. In spite of the large E-field confinement as observed on a nanometer scale, this doesn't affect the reproducibility in the SERS signals of the AgNWs@PTFE substrates (Figure S3b, Supporting Information) as a consequence of averaging the different hotspot responses within each acquisition laser spot.

As a second step toward the realization of SERS substrates for practical and rapid analytical testing, we devoted our further efforts in tailoring the SERS substrates in the form of spot arrays. The use of spots at constant surface area confining a sample drop there accommodated is primarily attracting because of the possibility to standardize the sample deposition and to perfect the reproducibility. Our choice of using laser ablation to pattern the AgNWs@PTFE substrate was mainly

motivated by: 1) a rapid and accurate texturing procedure and 2) the absence of additives needed as occurs in screen- or in ink jet-printing of nanomaterials. The latter require suitable organic media and stabilizing agents in adjusted amounts to sustain enough viscosity for uniform printing and to prevent edge-leakage or nozzles blockage, respectively.[13,44] Instead laser patterning promises a contaminant-free procedure that discards anomalous peaks from interfering in SERS spectra. Laser ablation is already being implemented in many industrial applications requiring engraving, cutting or cleaning such as microstructuring and drilling of electronic components, 3D-writing on glass, plastic and ceramic, removal of surface coating, etc.[45–47] Spots of a predefined diameter with in the 1 ÷ 2 mm range were initially obtained (Figure 1, step 2; Figure 4; Table S1 and Figures S4,5, Supporting Information) and their attitude towards influencing the evaporation behaviour of drying water drops was evaluated (Figure 5).

Different deposition and evaporation profiles were observed upon dropping a 5 μL water amount on the top of plain and patterned AgNWs@PTFE substrates tuned at the optimal AgNW density (*i.e.* 0.1 μg/mm^2). By adjusting the AgNW spot size to approach the diameter of the drop contact area on plain AgNWs@PTFE substrates (*i.e.* 2 mm in the case of 5 μL water drop), an increase of the contact angle from 100° to 118° of the as-deposited drop was observed (Figure 5a) and explained by a confinement of the drop within the surrounding PTFE hydrophobic barrier with consequent suppression of drop spreading. In this case the drop keeps an almost constant contact area even after complete evaporation to the opposite of what occurs in the case of pure PTFE and plain AgNWs@PTFE (Figure 5b). Concurrently the contact angle of the drying drop on the spot decreases regularly while occasional pinning with an irregular drop collapse characterizes plain AgNWs@PTFE substrates (Figure 5a).

Importantly different evaporation pathways are responsible for determining different distributions of the drop content, once evaporated. Specifically smaller contact angle values usually lead to larger deposition areas with lower and uneven molecular densities usually affected by "coffee-ring" deposits.[48] Conversely, when the liquid sample forms a high contact angle, the molecules are forced to gather within small areas upon evaporation and the deposition becomes more homogeneous.[49] Thus, starting contact angles as much as possible

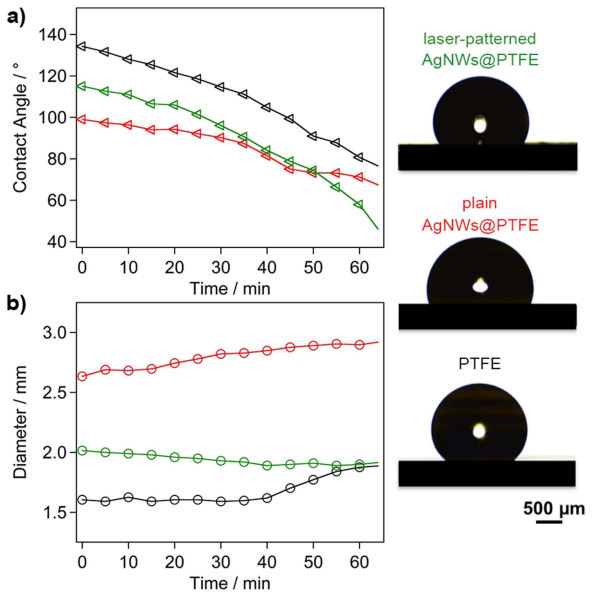

Figure 5. Contact angle (a) and diameter (b) values of a 5-μl water drop placed on pure PTFE (black line), plain AgNWs@PTFE substrate (red line) or a single spot of laser-patterned AgNWs@PTFE substrate (green line) at different times during drop drying at room temperature. Corresponding contact angle images of 5 μL water drops soon after deposition on pure PTFE, and on plain and spotted AgNWs@PTFE substrates are reported on the right. The AgNW density of the AgNWs@PTFE substrates was fixed at 0.1 μg/mm^2.

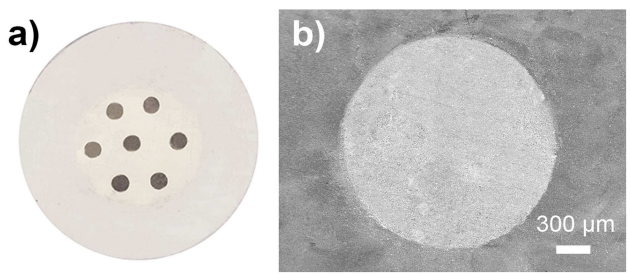

Figure 4. (a) Optical image of a laser-patterned AgNWs@PTFE substrate. (b) SEM image of a laser-patterned AgNWs@PTFE substrate centred on a single spot.

approaching the high-end values of pure PTFE as occurring in the case of the laser-patterned AgNWs@PTFE appear preferred to achieve reliable SERS measurements. The attempt to reduce the spot diameter below 2 mm at unvaried sample volume failed to further improve the SERS signal (not shown). In fact in this case the liquid overflows the spot edges and molecular deposits form in the peripheral PTFE area around the spot.

To investigate the benefits of confining sample drops within well-defined spots, we compared a SERS map of a protein deposition from a single plasmonic spot of the laser-patterned substrate with that obtained from the area occupied by a protein deposition in the case of a plain AgNWs@PTFE substrate (at the same 0.1 μg/mm^2 AgNW density). Compared to the latter where a coffee-ring distribution of deposited protein is apparent, in the laser-patterned substrate the molecules appear homogeneously covering the AgNWs spot area, with minimal fluctuations and maximal relative standard deviation (RSD) values not exceeding 10% (Figures 6a,b). We note that this scenario is lost when a twofold AgNW density spot is considered suffering from uneven signal distribution (Figure S6a, Supporting Information), which confirms again our initial observations (Figure 2) on the nanoparticle density of choice. A uniform molecular distribution is also beneficial to maximizing molecule/hotspot interactions leading to SERS spectra showing higher intensity values on average than in the case of the plain substrate (Figure 6c) and with enough signal down to submicromolar concentration values of protein (Figure S6b, Supporting Information).

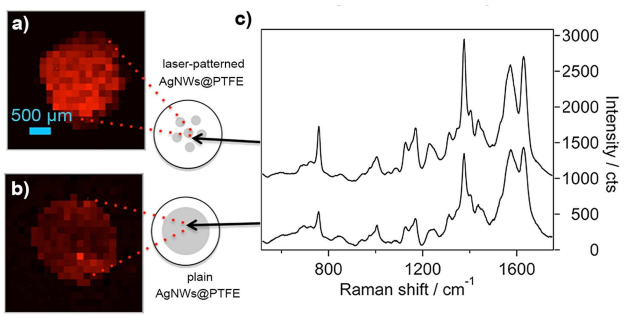

Figure 6. SERS maps ($\lambda_{ex}=532$ nm, 450 points, 150 μm step size) over a 5-μl drop deposition of Mb (1×10^{-6} M) on a single spot of a laser-patterned (a) or on a plain (b) AgNWs@PTFE substrate and resulting average spectra (c). The 1372 cm^{-1} (ν_4) band of Mb was considered for mapping. The RSD values referred to this peak are $\leq$10% and $\geq$15% for the laser-patterned AgNWs@PTFE and the plain AgNWs@PTFE substrates, respectively. The AgNW density of AgNWs@PTFE substrates was fixed at 0.1 μg/mm^2.

A quantitative estimate of the signal amplification provided by the laser-patterned AgNWs@PTFE substrates at the optimal Ag density was obtained by calculating the SERS enhancement factor EF. By considering the 1086 cm^{-1} peak from the SERS spectrum of 4-methylbenzenethiol (MBT), a common SERS probe forming self-assembled monolayers (SAM) on silver, and the 1372 cm^{-1} peak from the SERS spectrum of Mb (Figure S7, Supporting Information), EF values of 1×10^6 (MBT) and 6×10^5 (Mb), and 3×10^6 (MBT) and 9×10^5 (Mb), were obtained at $\lambda_{ex}=$ 532 and $\lambda_{ex}=785$ nm, respectively, which overcomes the enhancement capabilities of recently proposed SERS methods for biomolecule detection.[23,24,30]

Once clarified fundamental aspects regarding nanowire density and geometry to improve the signal gain of AgNWs@PTFE substrates, we tested them for practical and rapid analysis of biomolecules. The possibility to vary the excitation conditions throughout the visible-NIR range is of particular significance for both structural investigations and detection of biomolecules. For example, the heme group of Mb will mainly govern the SERS spectrum when operating in resonance conditions at 532 nm (Figures 2,6) while signals belonging to the peptide backbone and amino acid side chains are revealed when a 785 nm is used (Figure 7a, Table S2, Supporting Information for peak assignments). In general, longer excitation wavelengths are usually preferred for Raman-based diagnostics to avoid the superposition of heme bands as well as background fluorescence usually affecting many biological samples when operating at excitation wavelengths below 700 nm.[50]

The flexibility of the spotted AgNWs@PTFE substrate is here further demonstrated by SERS detection of larger proteins, specifically the hemoprotein catalase ($M_w=250$ kDa) and bovine serum albumin (BSA, $M_w=68$ kDa) (Tables S3,4, Supporting Information for peak assignments), whose SERS identification previously proved not trivial at low concentration values,[51–53] mainly because of their large molecular size leading to a variable nano-bio interface.[54–56] Sharp bands were obtained for both proteins. The SERS spectrum of catalase (Figure 7b) under out-of-resonance conditions (at $\lambda_{ex}=785$ nm) is less affected by the high cross-section bands of the heme

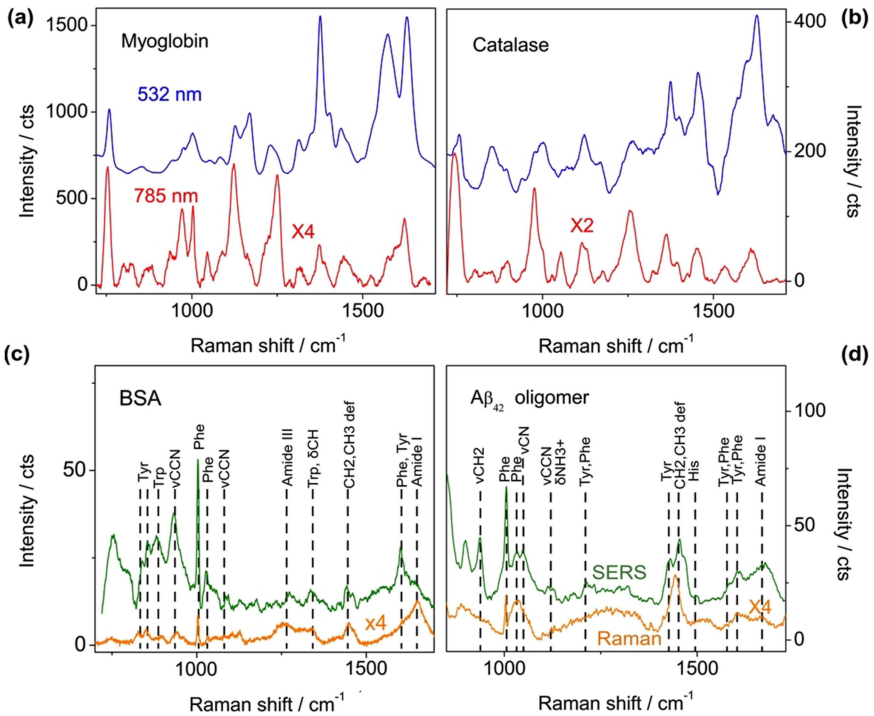

Figure 7. SERS spectra of Mb (a) and catalase (b) at 1×10^{-6} M under $\lambda_{ex}=532$ nm (blue) and $\lambda_{ex}=785$ nm (red) deposited on laser-patterned AgNWs@PTFE. SERS spectra (green) of BSA (c) and $A\beta_{42}$ oligomer (d) at 1×10^{-6} M under $\lambda_{ex}=785$ nm deposited on laser-patterned AgNWs@PTFE. Raman spectra (orange) of 1×10^{-3} M BSA and $A\beta_{42}$ oligomer are also shown as reference.

group as similarly noted for Mb, revealing modes ascribed to aminoacid residues (Table S2). In the case of BSA (Figure 7c), characteristic vibrations of aromatic aminoacid at 838/855 cm^{-1} (Tyr), 880 cm^{-1} (Trp), 1003/1027 cm^{-1} (Phe) and 1601 cm^{-1} (Phe, Tyr) as well as to the peptide backbone and aliphatic residues at 1270 cm^{-1} (Amide III), 1445 cm^{-1} (CH_2, CH_3 deformations) and 1651 cm^{-1} (Amide I) are visible in the Raman spectrum and accordingly identified in the SERS spectrum.

We finally performed a SERS characterization on amyloid aggregates, which show a marked heterogeneity and metastability complicating their structural analysis by standard structural biology techniques,[57] as well as by spectroscopic methods, including plasmon-enhanced spectroscopies.[58–62] Figure 7d shows the on-spot SERS spectrum obtained by drop deposition on a AgNWs@PTFE substrate of β-amyloid peptide $A\beta_{42}$ oligomers (see Table S5, Supporting Information for peak assignments), which are associated with Alzheimer's disease (AD) and a well recognised biomarker of the cerebrospinal fluid of AD patients. Here, strong peaks emerge in the SERS spectrum: 940 cm^{-1} (ν_{CH2}), 1003 and 1030 cm^{-1} (Phe), 1049 cm^{-1} (ν_{CN}), 1454 cm^{-1} ($\delta_{CH2,CH3}$) and 1605 cm^{-1} (Tyr, Phe) while less intense spectral features are observed at 1115 and 1126 cm^{-1} (ν_{CCN}, δ_{NH3+}), 1430 cm^{-1} (Tyr), 1498 cm^{-1} (His) and 1582 cm^{-1} (Tyr, Phe). Considerations on relative peak intensities and comparison between Raman and SERS spectral features may also prove useful to gaining insights into surface structuring of the biomolecule. For example, matching Raman and SERS bands of BSA may suggest that the protein structure is negligibly affected by the interaction with the AgNWs, even if prevailing peaks at 1003 cm^{-1} and 1601 cm^{-1} represent an indication of Phe and Tyr residues spatially near the hotspots. Analogously, the anomalous intensities associated with aromatic, aliphatic and N-containing groups of $A\beta_{42}$ oligomers with respect to their counterpart in the reference Raman spectrum let entail that both electrostatic (by amino groups) and hydrophobic (by aliphatic and aromatic residues) interactions are established with the silver and/or that both charged and hydrophobic aminoacid residues are in direct proximity with the metal, and thus exposed on the amyloid surface.

3. Conclusion

A novel strategy of SERS assay for rapid and effective detection as well as for simple structural characterization of biomolecules is presented. In our scheme, by implementing a mixed bottom-up/top-down approach, dot arrays of AgNWs clustered on hydrophobic supports are obtained and proven as efficient sensing SERS substrates for catching the analyte content from a minute amount of liquid sample and its rapid SERS inspection. By a simple flow-through method, AgNWs assemblies stuffed with interstitial hotspots are rapidly realized. Afterwards, laser ablation is exploited to operate a substrate patterning in the form of regular SERS-active spots producing intense local E-fields. The system overcomes the issues typically encountered with aggregating metal colloids, which suffer from scarce standardization perspectives. Overall, our attempts may represent a concrete chance for progressing SERS toward widespread commercially viable sensing applications including diagnostics at the point-of-need settings and on-site analyses.

Experimental Section

Materials

Ethylene glycol (EG, 99%) was obtained from Scharlab. Polyvinyl pyrrolidone (PVP, M_w 40000), $AgNO_3$, AgCl, isopropanol (99.5%) and ethanol (≥99.8%) were purchased from Sigma-Aldrich. Hydrophobic (25 mm diameter × 80 μm thickness) PTFE filter membranes of 0.45 μm pore size by Sartorius were used. Mb from human heart, BSA and catalase from bovine liver were obtained from Sigma-Aldrich and used as received. $A\beta_{42}$ oligomers were prepared as previously described.[63]

AgNWs Synthesis

AgNWs (1.5 ± 0.9 μm in length, 78 ± 16 nm in diameter) were synthesized by the chemical reduction method of silver nitrate in EG and PVP, according to Hu et al.[64] with minor changes. Briefly, in one liter round bottom flask, 3.0 g of PVP were added and dissolved in 180 ml of EG in few hours. After the complete dissolution, the solution was heated up at 170 °C. To this flask, 225 mg of AgCl were added and after 3 min a solution of $AgNO_3$ (990 mg of $AgNO_3$ in 20 ml of EG) was also dropped inside during a 10 min time (2 ml/min). The reaction proceeded for additional 30 min at 170 °C. After 30 min, the light-grey suspension was cooled down in ice water bath. The suspension was 3 times washed with acetone and the AgNWs were precipitated by centrifugation (3000 rpm, 15 min). The purified nanowires were finally suspended in isopropanol and characterized by SEM (Zeiss, EVO MA 10) and UV-Vis spectroscopy (PerkinElmer Lambda 35 UV/Vis) (Figure S1, Supporting Information).

Arrays Fabrication

The initial suspension of AgNWs (Ag 0.017 wt%) was diluted in different ratios in ethanol. An amount of 2 mL of solution was then passed through the PTFE membrane by using an Amicon Stirred cell Model 8003, 3 ml (Millipore) cell. Specifically the membrane was initially wetted by dipping it in ethanol and then placed into the filter holder. Then the AgNW solution was filtered by adjusting the pressure at an optimized value of 350 mbar. The substrate was then extensively washed in anhydrous ethanol and there stored until further use. Part of the as-fabricated substrates was finally patterned in the form of dot arrays by using a laser ablation procedure. Briefly, as the AgNWs have a considerable absorption coefficient (of the order of 10^5 cm^{-1}) in the blue-green spectral region, the substrates were processed by using the second harmonic (532 nm) of a Q-Switch Nd:YAG laser (10 ns pulse duration). The fiber-coupled laser output was lens-imaged to form a spot of 2.5 mm diameter on the sample plane. The beam radii ω_0 was precisely determined by applying the spot regression method for Gaussian laser beam profiles (Figure S4, Supporting Information). A custom designed mask, composed of round metal rods (within the 1 ÷ 2 mm diameter range), was positioned onto the AgNWs layer to shield incoming laser light and create dot arrays. To minimize undesired thermal effects of PTFE membrane, array fabrication was performed by full immersion in a glass cell containing ethanol. Then, laser patterning was performed by scanning in orthogonal directions at fluence values slightly above

the AgNWs single-pulse ablation threshold fluence (Table S1, Supporting Information). The optimal removal window for surface densities between 0.1 and 0.4 μg/mm^2 was found to be in the 160–250 mJ cm^{-2} range. Thus, 160–180 mJ cm^{-2}, 2 Hz pulse repetition frequency and full immersion in ethanol were selected as the best parameters to pattern the AgNWs@PTFE substrates used in the SERS experiments of this work. The morphology of the laser-patterned AgNWs@PTFE substrates was inspected by tapping mode AFM by using a JPK NanoWizard III Sense scanning probe microscope at 250÷300 kHz drive frequency and 0.5 Hz scan rate and equipped with single beam uncoated silicon cantilevers (μMash HQ:NSC15 Cr–Au BS). Contact angle measurements were conducted under a home made set up by placing a 5-μL aqueous droplet onto the AgNWs@PTFE substrate and following the drop evolution during its evaporation. The method used for FEM modeling is described in Supporting Information.

SERS Measurements

SERS measurements were carried out using a microRaman spectrometer (Xplora, Horiba) working at 532 nm or 785 nm laser wavelengths with a 1200 grooves/mm grating. The backscattered light was collected by a 10×objective with 0.25 NA, which generates a 7-μm large laser beam waist and provides an average SERS response, minimizing possible signal variability. Laser power values at the sample of 115 μW at 532 nm and 598 μW at 785 nm and an integration time of 10 s with two accumulations were used. SERS data are baseline corrected and represent an average of a minimum of 10 spectra collected by mapping experiments over 12 mm^2 areas with a step size of 50÷150 μm, unless specified otherwise.

Supporting Information

Supporting Information is available from the Wiley Online Library or from the author.

Acknowledgements

M.B., C.D'A., M.deA., R.P. and P.M. acknowledge support from the European Community and the Ministry of Education, University and Research of Italy (MIUR) through the ERANET EuroNanoMed III "Surface-enhanced Raman scattering with nanophotonic and biomedical amplifying systems for an early diagnosis of Alzheimer's disease pathology" SPEEDY project (ID 221) and from the Ministry of Foreign Affairs and International Cooperation of Italy (MAECI) through the "Development of a cost-effective wearable metal nanowire-based chip sensor for optical monitoring of metabilites in sweat" DESWEAT project (n° KR19GR08) funded within the frame of the Executive Programme of Scientific and Technological Cooperation between the Italian Republic and the Korean Republic 2019–2021.

Conflict of Interest

The authors declare no conflict of interest.

Keywords: biomolecules · laser patterning · amyloids · plasmonic nanoparticles · label-free detection

[1] P. L. Stiles, J. A. Dieringer, N. C. Shah, R. P. Van Duyne, *Annu. Rev. Anal. Chem (Palo Alto, Calif.)* **2008**, *1*, 601.
[2] H. Liu, L. Yang, J. Liu, *TrAC Trends Anal. Chem.* **2016**, *80*, 364.
[3] R. A. Alvarez-Puebla, L. M. Liz-Marzan, *Chem. Soc. Rev.* **2012**, *41*, 43.
[4] J. F. Betz, W. W. Yu, Y. Cheng, I. M. White, G. W. Rubloff, *Phys. Chem. Chem. Phys.* **2014**, *16*, 2224.
[5] Y. Wang, Y. Jin, X. Xiao, T. Zhang, H. Yang, Y. Zhao, J. Wang, K. Jiang, S. Fan, Q. Li, *Nanoscale* **2018**, *10*, 15195.
[6] J. W. Liu, J. L. Wang, W. R. Huang, L. Yu, X. F. Ren, W. C. Wen, S. H. Yu, *Sci. Rep.* **2012**, *2*, 987.
[7] X. Li, H. K. Lee, I. Y. Phang, C. K. Lee, X. Y. Ling, *Anal. Chem.* **2014**, *86*, 10437.
[8] J. Kneipp, H. Kneipp, K. Kneipp, *Chem. Soc. Rev.* **2008**, *37*, 1052.
[9] M. Prochazka, Surface-Enhanced Raman Spectroscopy: Bioanalytical, Biomolecular and Medical Applications. In *Surface-Enhanced Raman Spectroscopy: Bioanalytical, Biomolecular and Medical Applications*, **2016**, pp 1–221.
[10] S. Abalde-Cela, P. Aldeanueva-Potel, C. Mateo-Mateo, L. Rodriguez-Lorenzo, R. A. Alvarez-Puebla, L. M. Liz-Marzan, *J. R. Soc. Interface* **2010**, *7 Suppl 4*, S435.
[11] W. R. Premasiri, Y. Chen, J. Fore, A. Brodeur, L. D. Ziegler, Chapter 10 – SERS biomedical applications: diagnostics, forensics, and metabolomics. In *Frontiers and advances in molecular spectroscopy*, J. Laane, Ed. Elsevier: **2018**, pp 327–367.
[12] W. W. Yu, I. M. White, *Anal. Chem.* **2010**, *82*, 9626.
[13] L. L. Qu, D. W. Li, J. Q. Xue, W. L. Zhai, J. S. Fossey, Y. T. Long, *Lab Chip* **2012**, *12*, 876.
[14] M. J. Oliveira, P. Quaresma, M. Peixoto de Almeida, A. Araujo, E. Pereira, E. Fortunato, R. Martins, R. Franco, H. Aguas, *Sci. Rep.* **2017**, *7*, 2480.
[15] W. Wu, L. Liu, Z. Dai, J. Liu, S. Yang, L. Zhou, X. Xiao, C. Jiang, V. A. Roy, *Sci. Rep.* **2015**, *5*, 10208.
[16] L. Polavarapu, A. L. Porta, S. M. Novikov, M. Coronado-Puchau, L. M. Liz-Marzan, *Small* **2014**, *10*, 3065.
[17] I. Bruzas, W. Lum, Z. Gorunmez, L. Sagle, *Analyst* **2018**, *143*, 3990.
[18] D. Cialla-May, X. S. Zheng, K. Weber, J. Popp, *Chem. Soc. Rev.* **2017**, *46*, 3945.
[19] D. Kurouski, M. Sorci, T. Postiglione, G. Belfort, I. K. Lednev, *Biotechnol. Prog.* **2014**, *30*, 488.
[20] I. D. G. Macdonald, W. E. Smith, *Langmuir* **1996**, *12*, 706.
[21] X. Dou, Y. M. Jung, Z.-Q. Cao, Y. Ozak, *Appl. Spectrosc.* **1999**, *53*, 1440.
[22] M. I. Stockman, *Phys. Today* **2011**, *64*, 39.
[23] P. Matteini, M. Cottat, F. Tavanti, E. Panfilova, M. Scuderi, G. Nicotra, M. C. Menziani, N. Khlebtsov, M. de Angelis, R. Pini, *ACS Nano* **2017**, *11*, 918.
[24] B. Fazio, C. D'Andrea, A. Foti, E. Messina, A. Irrera, M. G. Donato, V. Villari, N. Micali, O. M. Marago, P. G. Gucciardi, *Sci. Rep.* **2016**, *6*.
[25] J. H. Granger, N. E. Schlotter, A. C. Crawford, M. D. Porter, *Chem. Soc. Rev.* **2016**, *45*, 3865.
[26] H. Marks, M. Schechinger, J. Garza, A. Locke, G. Coté, *Nanophotonics* **2017**, *6*, 681.
[27] K. Kneipp, A. S. Haka, H. Kneipp, K. Badizadegan, N. Yoshizawa, C. Boone, K. E. Shafer-Peltier, J. T. Motz, R. R. Dasari, M. S. Feld, *Appl. Spectrosc.* **2002**, *56*, 150.
[28] S. A. Meyer, E. C. Le Ru, P. G. Etchegoin, *J. Phys. Chem. A* **2010**, *114*, 5515.
[29] N. Feliu, M. Hassan, E. G. Rico, D. X. Cui, W. Parak, R. Alvarez-Puebla, *Langmuir* **2017**, *33*, 9711.
[30] M. Banchelli, M. de Angelis, C. D'Andrea, R. Pini, P. Matteini, *Sci. Rep.* **2018**, *8*, 1033.
[31] S. Yang, X. Dai, B. B. Stogin, T. S. Wong, *Proc. Natl. Acad. Sci. USA* **2016**, *113*, 268.
[32] P. Matteini, M. de Angelis, L. Ulivi, S. Centi, R. Pini, *Nanoscale* **2015**, *7*, 3474.
[33] F. De Angelis, F. Gentile, F. Mecarini, G. Das, M. Moretti, P. Candeloro, M. L. Coluccio, G. Cojoc, A. Accardo, C. Liberale, R. P. Zaccaria, G. Perozziello, L. Tirinato, A. Toma, G. Cuda, R. Cingolani, E. Di Fabrizio, *Nat. Photonics* **2011**, *5*, 682.
[34] W. Z. Li, W. Wei, J. Y. Chen, J. X. He, S. N. Xue, J. Zhang, X. Liu, X. Li, Y. Fu, Y. H. Jiao, K. Zhang, F. Liu, E. H. Han, *Nanotechnology* **2013**, *24*, 105302.

[35] M. Chen, I. Y. Phang, M. R. Lee, J. K. Yang, X. Y. Ling, *Langmuir* **2013**, *29*, 7061.
[36] M. N'Gom, J. Ringnalda, J. F. Mansfield, A. Agarwal, N. Kotov, N. J. Zaluzec, T. B. Norris, *Nano Lett.* **2008**, *8*, 3200.
[37] P. van der Wal, U. Steiner, *Soft Matter* **2007**, *3*, 426.
[38] L.-Q. Lu, Y. Zheng, W.-G. Qu, H.-Q. Yu, A.-W. Xu, *J. Mater. Chem.* **2012**, *22*, 20986.
[39] S. Hu, K. M. Smith, T. G. Spiro, *J. Am. Chem. Soc.* **1996**, *118*, 12638.
[40] D. A. Clayton, T. E. McPherson, S. Pan, M. Chen, D. A. Dixon, D. Hu, *Phys. Chem. Chem. Phys.* **2013**, *15*, 850.
[41] S. R. Panikkanvalappil, N. Hooshmand, M. A. El-Sayed, *Bioconjugate Chem.* **2017**, *28*, 2452.
[42] A. R. Tao, P. Yang, *J. Phys. Chem. B* **2005**, *109*, 15687.
[43] T. Hutter, S. R. Elliott, S. Mahajan, *Nanotechnology* **2013**, *24*, 035201.
[44] D. J. Finn, M. Lotya, J. N. Coleman, *ACS Appl. Mater. Interfaces* **2015**, *7*, 9254.
[45] S. Mishra, V. Yadava, *Opt. Laser Eng.* **2015**, *73*, 89.
[46] M. Malinauskas, A. Zukauskas, S. Hasegawa, Y. Hayasaki, V. Mizeikis, R. Buividas, S. Juodkazis, *Light Sci Appl* **2016**, *5*, e16133.
[47] S. Siano, R. Salimbeni, *Acc. Chem. Res.* **2010**, *43*, 739.
[48] R. D. Deegan, O. Bakajin, T. F. Dupont, G. Huber, S. R. Nagel, T. A. Witten, *Nature* **1997**, *389*, 827.
[49] R. G. Larson, *AIChE J.* **2014**, *60*, 1538.
[50] S. Yang, B. Li, M. N. Slipchenko, A. Akkus, N. G. Singer, Y. N. Yeni, O. Akkus, *J. Raman Spectrosc.* **2013**, *44*, 1089.
[51] K. Wongravee, H. Gatemala, C. Thammacharoen, S. Ekgasit, S. Vantasin, I. Tanabe, Y. Ozaki, *RSC Adv.* **2015**, *5*, 1391.
[52] L. Zhang, C. Guan, Y. Wang, J. Liao, *Nanoscale* **2016**, *8*, 5928.
[53] W. Huttner, K. Christou, A. Gohmann, V. Beushausen, H. Wackerbarth, *Microfluid. Nanofluid.* **2011**, *12*, 521.
[54] X. X. Han, H. Y. Jia, Y. F. Wang, Z. C. Lu, C. X. Wang, W. Q. Xu, B. Zhao, Y. Ozaki, *Anal. Chem.* **2008**, *80*, 2799.
[55] E. S. Grabbe, R. P. Buck, *J. Am. Chem. Soc.* **1989**, *111*, 8362.
[56] X. Gu, Y. Yan, G. Jiang, J. Adkins, J. Shi, G. Jiang, S. Tian, *Anal. Bioanal. Chem.* **2014**, *406*, 1885.
[57] F. Chiti, C. M. Dobson, *Annu. Rev. Biochem.* **2017**, *86*, 27.
[58] R. Buividas, N. Dzingelevicius, R. Kubiliute, P. R. Stoddart, T. Vi Khanh, E. P. Ivanova, S. Juodkazis, *J. Biophotonics* **2015**, *8*, 567.
[59] V. Voiciuk, G. Valincius, R. Budvytyte, A. Matijoska, I. Matulaitiene, G. Niaura, *Spectrochim Acta A Mol Biomol Spectrosc* **2012**, *95*, 526.
[60] D. Bhowmik, K. R. Mote, C. M. MacLaughlin, N. Biswas, B. Chandra, J. K. Basu, G. C. Walker, P. K. Madhu, S. Maiti, *ACS Nano* **2015**, *9*, 9070.
[61] Y. Kim, J. H. Park, H. Lee, J. M. Nam, *Sci. Rep.* **2016**, *6*, 19548.
[62] C. D'Andrea, A. Foti, M. Cottat, M. Banchelli, C. Capitini, F. Barreca, C. Canale, M. de Angelis, A. Relini, O. M. Marago, R. Pini, F. Chiti, P. G. Gucciardi, P. Matteini, *Small* **2018**, *14*, e1800890.
[63] A. R. A. Ladiwala, J. Litt, R. S. Kane, D. S. Aucoin, S. O. Smith, S. Ranjan, J. Davis, W. E. Van Nostrand, P. M. Tessier, *J. Biol. Chem.* **2012**, *287*, 24765.
[64] L. Hu, H. S. Kim, J. Y. Lee, P. Peumans, Y. Cui, *ACS Nano* **2010**, *4*, 2955.

Manuscript received: January 16, 2018
Version of record online: ■■, ■■■

FULL PAPER

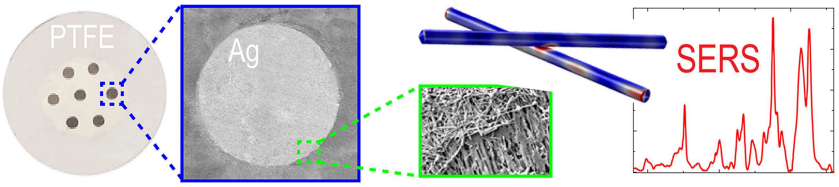

In the spotlight: By implementing a mixed bottom-up/top-down approach, dot arrays of AgNWs clustered on hydrophobic supports are obtained and proven as efficient sensing surface-enhanced Raman scattering (SERS) substrates for catching the analyte content from a minute amount of liquid sample and performing rapid SERS inspection.

*Dr. M. Banchelli, Dr. C. Amicucci, Dr. E. Ruggiero, Dr. C. D'Andrea, Dr. M. Cottat, Dr. D. Ciofini, Dr. I. Osticioli, Dr. G. Ghini, Dr. S. Siano, Prof. R. Pini, Dr. M. de Angelis, Dr. P. Matteini**